Delft University of Technology

Delft Center for Systems and Control

Technical report 21-009

Model predictive control for optimal integration of a thermal chimney and solar shaded building*

T.J. Ceha, L.A. de Araujo Passos, S. Baldi, and B. De Schutter

If you want to cite this report, please use the following reference instead:
T.J. Ceha, L.A. de Araujo Passos, S. Baldi, and B. De Schutter, "Model predictive control for optimal integration of a thermal chimney and solar shaded building," *Proceedings of the 2021 29th Mediterranean Conference on Control and Automation (MED)*, Bari, Italy, pp. 21–26, June 2021. doi:10.1109/MED51440.2021.9480299

Delft Center for Systems and Control
Delft University of Technology
Mekelweg 2, 2628 CD Delft
The Netherlands
phone: +31-15-278.24.73 (secretary)
URL: https://www.dcsc.tudelft.nl

*This report can also be downloaded via https://pub.bartdeschutter.org/abs/21_009.html

Model Predictive Control for Optimal Integration of a Thermal Chimney and Solar Shaded Building*

Thomas Joseph Ceha, Luigi Antonio de Araujo Passos, Simone Baldi, and Bart De Schutter

Abstract— **Energy-saving devices are extensively sought in several fields, including heating, ventilation, and air-conditioning (HVAC) tasks in buildings. This paper investigates six model predictive control (MPC) strategies as a way to optimize the operation of a solar shaded, natural ventilated building located at TU Delft campus. Such building is based on an innovative combination of a thermal chimney and glazing walls for harvesting passive energy. The main challenge is dealing with the system dynamics. The predictive controllers we consider include both linear and nonlinear MPC, and four hierarchical MPC strategies. All controllers aim to minimize auxiliary power consumption and, consequently, increasing the energy savings. The six control strategies performance are evaluated using reference values for thermal comfort, while relying on simulations performed in MATLAB for calculations. The hierarchical MPC architecture which considers a hybrid structure with nonlinear tracker for ventilation and linear agents for heating purposes appears the most promising one.**

I. Introduction

As the quest for energy efficiency is trending now, several innovative technologies have been proposed for HVAC (Heating, Ventilation, and Air-Conditioning) in buildings. This is because of the high energy consumption in indoor spaces, which, for instance, reaches half of the total energy consumption in European Union [1]. The HVAC solutions considered mostly rely on passive systems, renewable energy sources, and efficient processes/devices, e.g., steerable solar shadings, smart windows, thermal chimneys, phase-change materials (PCM), and photovoltaic panels [2].

While these systems are mainly driven by unsteady weather conditions, the development of operational control strategies plays an essential role for achieving the best system performance and energy dispatchability. Such operational strategies rely on control algorithms and optimization methods for establishing optimal decisions and to assess relevant figures of merit (energy savings, thermal comfort levels, ventilation rates, etc.). MPC (Model Predictive Control) has demonstrated to be a promising method for energy management in buildings [3]. Many MPC variants have been considered in the literature, e.g., robust, adaptive schemes [4], scenario-based stochastic control [5], off-line distributed MPC [6], and stochastic MPC [7]. In addition, multiple control structures have been compared, such as centralized, decentralized, distributed, and hierarchical MPC controllers [8-10], often concluding that the last two are superior in performance and computational efforts, depending on the complexity of the building. Some examples of analysis may include controlling the thermal stratification in shopping malls [11], air flows in libraries [12], and nighttime ventilation in office buildings [13].

In this work, we aim to develop and compare a set of MPC strategies to optimize the operation of a novel HVAC system installed in a living lab office-building based at TU Delft campus, in the Netherlands. Such system relies on the combination of a thermal chimney and glazed shaded walls, while considering PCM for latent thermal storage. While different MPC approaches have been suggested for buildings equipped with active HVAC systems, such control method has not been investigated for this combination of passive actuators for heating and ventilation. Therefore, the analysis explores six different MPC architectures to systematically operate the system actuators, which consist of the thermal chimney flow area and the solar shadings aperture. The control algorithms rely on a fully transient thermal model numerically implemented in MATLAB to explore different control strategies in order to guarantee the maximum passive fraction, and, consequently, the minimum use of auxiliary heating.

II. System description and dynamic modeling

A. Building and HVAC system configuration

The thermal system of this study is currently installed at TU Delft in a space particularly designed for testing passive technologies in co-working conditions. Figure 1 shows the schematic representation. As one can see, the configuration shown in Figure 1 includes a thermal chimney, in which the stack effect due to buoyancy provides natural ventilation, and a fully glazed walls building, where the solar heat gain coming into the place is controlled by external shades. Additionally, the chimney is supported by an auxiliary heater and PCM battery for thermal buffering. Therefore, the system mainly relies on the combination of passive technologies (i.e., thermal chimney and solar shadings) to meet indoor thermal comfort requirements, in which an optimal controller should contribute to a satisfactory performance. The building space is designed to support up to 240 people and the activities performed include meetings, presentations, and office work. Regarding the operation modes, the building is open for occupancy every day, in a time schedule from 8

* Research supported by the Netherlands Enterprise Agency (RVO) CONVERGE Project TEUE318008.

Thomas Joseph Ceha, Luigi Antonio de Araujo Passos, and Bart De Schutter are with the Delft Center for Systems and Control, Faculty of Mechanical, Maritime and Materials Engineering, Delft University of Technology, Delft, 2628CD, Netherlands (e-mail: thom_ceha@hotmail.com, l.a.dearaujopassos@tudelft.nl, b.deschutter@tudelft.nl).

Simone Baldi (corresponding author) is with the School of Mathematics, Southeast University, Nanjing, 210096, China (email: s.baldi@tudelft.nl).

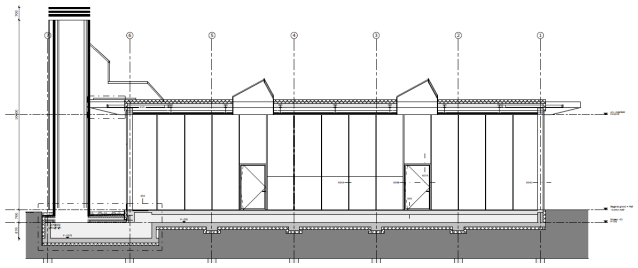

Fig. 1: Building and HVAC system layout

TABLE I: Dimensions and materials where V means volume, ρ specific mass, C specific heat and ε thermal emissivity.

Section	Material	V [m^3]	ρ [kg/m^3]	C [J/kg/K]	ε [–]
N-S walls	Low-e glass	2.11	2470	900	0.86[a]
E-W walls	Low-e glass	3.51	2470	900	0.86[a]
Roof	Bitumen	1.22	1050	1800	0.93
Ceiling	Galvanized steel	0.46	7850	500	0.23
Floor	Concrete	75.94	2000	840	0.60
Room	Air	1579.5	1	1000	-

[a] The value of 0.2 is considered on the internal side of the glasses.

a.m. to 4 p.m. Therefore, thermal comfort is only relevant to be achieved during those hours.

The building dimensions, materials and thermal-physical properties considered, are shown in Table I. The theoretical values are obtained by means of the technical database CES EduPack [14].

B. Thermal modeling

The physical system introduced in Figure 1 is mathematically modeled according to the principles of conservation of energy and heat transfer [15]. The data is provided at discrete time instant $t^k = k\Delta t$, in which Δt is the sample time. Therefore, the air flow rates coming across the building at the time step k is expressed as follows:

$$\dot{m}^k = \rho^k C_{\mathrm{D}} \phi \hat{u}_{\mathrm{v}}^k \sqrt{2gH \frac{|T_{\mathrm{i}}^k - T_{\mathrm{o}}^k|}{T_{\mathrm{o}}^k}} \tag{1}$$

where C_{D} refers to a nondimensional discharge coefficient, ϕ is the chimney's flow area, $\hat{u}_{\mathrm{v}}^k$ is the control input for optimal flow area fraction, g the gravitational constant, H the chimney height, ρ^k the air specific mass, and T_{i}^k and T_{o}^k refer to the temporal indoor and outdoor air temperatures, respectively. One should note that (1) assumes incompressible flow (and disregards friction losses). Therefore, the time variance of ambient temperature guarantees the variation of flowrate. In addition, the coefficient C_{D} is fixed to 0.62, based on calibrations with CFD simulations, while regarding the tower dimensions, $\phi = 4\,\mathrm{m}^2$ and $H = 4\,\mathrm{m}$.

For determining the evolution of the indoor temperature along time, an energy balance is applied to the fluid volume considered and to the 6 solid surfaces of the building (i.e., s_1 for the ceiling, s_2-s_5 for the walls, and s_6 for the floor). The fluid modeling mainly assumes a full-mixed temperature node inside the building (i.e., the air temperature inside the building is uniform along the space and it is only a function of time), so the temporal heat interaction regarding the air indoor and its surroundings is expressed as:

$$T_{\mathrm{i}}^k = T_{\mathrm{i}}^{k-1} + (\dot{q}_{\mathrm{p}}^k - \dot{q}_{\mathrm{v}}^k - \dot{q}_{\mathrm{ci}}^k) \frac{\Delta t}{M_{\mathrm{i}} C_{\mathrm{i}}} \tag{2}$$

where $\dot{q}_{\mathrm{p}}^k$ refers to internal heat gain from occupants, $\dot{q}_{\mathrm{v}}^k$ is the indoor ventilation rate, and $\dot{q}_{\mathrm{ci}}^k$ the total convective heat transfer between the air and bordering solids. Moreover, M_{i} refers to the mass of air, and C_{i} to the specific heat at constant pressure. The heat transfer rates considered in (2) are:

$$\dot{q}_{\mathrm{p}}^k = 100(P^k) \tag{2.1}$$

$$\dot{q}_{\mathrm{v}}^k = \dot{m}^k C_{\mathrm{i}} (T_{\mathrm{i}}^k - T_{\mathrm{o}}^k) \tag{2.2}$$

$$\dot{q}_{\mathrm{ci}}^k = \sum_{s=\mathrm{s}_1}^{\mathrm{s}_6} \dot{q}_{\mathrm{c},s}^k \tag{2.3}$$

where s_1-s_6 refers to the corresponding solid surfaces, P^k refers to the number of people inside the building, and $\dot{q}_{\mathrm{c},s}^k$ is the individual convective heat transfer for each solid surface. Note that the number 100, included in (2.1), refers to the metabolic heat generation per person. For determining the solid temperatures, a general energy balance for all surfaces results in the following expression:

$$T_s^k = T_s^{k-1} + (\widehat{U}_s^k \dot{q}_{\mathrm{s},s}^k - \dot{q}_{\mathrm{r},s}^k - \dot{q}_{\mathrm{c},s}^k - \dot{q}_{\mathrm{d},s}^k) \frac{\Delta t}{M_s C_s} \tag{3}$$

where $\widehat{U}_s^k$ is the control input set for optimal shadings aperture, $\dot{q}_{\mathrm{s},s}^k$ is the solar heat rate, $\dot{q}_{\mathrm{r},s}^k$ the radiative heat rate and $\dot{q}_{\mathrm{d},s}^k$ the conductive heat rate, while M_s refers to the solid mass, and C_s the specific heat of the respective solid considered. It is important to mention that when considering the ceiling (i.e., $s = \mathrm{s}_1$, $\widehat{U}_{\mathrm{s}_1}^k = 1$, since there is no shading over the roof. Moreover, the heat rates between the brackets, in (3), depend on the kind of solid considered. Therefore,

$$\dot{q}_{\mathrm{s},s}^k = I^k A_s \tau_s \alpha_s \tag{3.1}$$

$$\dot{q}_{\mathrm{r},s}^k = \frac{\sigma A_s \varepsilon_s \left[\left(T_s^k\right)^4 - \left(T_{\mathrm{o}}^k - 8\right)^4 \right]}{F_{1-2}} \tag{3.2}$$

$$\dot{q}_{\mathrm{c},s}^k = h_s^k A_s \left(T_s^k - T_{\mathrm{o}}^k\right) \tag{3.3}$$

$$\dot{q}_{\mathrm{d},s}^k = \lambda_s A_s (T_s^k - T_{\mathrm{g}}^k) \tag{3.4}$$

where I^k refers to the solar radiation incidence, τ_s refers to transmittance, α_s to absorptance, ε_s the thermal emissivity, σ the radiative constant, F_{1-2} the radiative view factor, h_s^k the convective coefficient, λ_s the thermal conductivity, and T_{g}^k the ground temperature. At this moment, it is important to mention other assumptions regarding (3). For instance, when dealing with the ceiling (s_1) and the floor (s_6), $\dot{q}_{\mathrm{r},s}^k = 0$. On

the other hand, $\dot{q}^k_{\mathrm{d},s} = 0$ in the walls (s_2-s_5). Additionally, T^k_{g} in (3.4) denotes the roof temperature when using (3) for the ceiling (s_1). In this paper, the convective coefficients are calculated according to the solid geometry, fluid velocity, and thermal-physical properties, such as thermal conductivity, specific mass and viscosity, generally written in terms of non-dimensional numbers [15]. On the other hand, the view factor $F_{1-2} = 1$ for external surfaces and $F_{1-2} = 2 - \varepsilon_s$ for enclosure surfaces [15]. For predicting ground temperatures, a plain cosines model is developed, based on ground data from the Royal Dutch Meteorological Institute [16].

For modeling the weather conditions acting as system disturbance, i.e., ambient temperature, solar irradiance, and wind velocity, TMY (Typical Meteorological Year) data for Amsterdam is considered. One should note that the radiation values typically provided by weather databases account only measurements at the horizontal and at a solar-tracked surface. In this case, I^k is particularly accounted for each surface considering the vertical tilting, orientation, solar angles, and Perez model for diffuse components, as fully described in [17]. However, for simplicity, such details will not be covered in this paper (see [17] for more details).

III. Control Architecture

While the system under consideration contains variable energy sources (i.e., solar and buoyancy), the HVAC design includes active components that may be controlled in order to provide effective energy management. For instance, the shadings aperture area determines solar heat gains, the chimney flow aperture form the ventilation rates across the building, etc. Hence, the challenge is to find optimal control signals for these actuators, while sufficiently suppressing the computation time for on-line application. Six distinct MPC architectures are analyzed to tackle this challenge.

The two single-level MPC architectures implemented in this work consider linear and nonlinear modeling approaches. In addition, four hierarchical MPC structures are introduced, employing a linear MPC reference determining agent and a nonlinear MPC reference tracker slave. Since the thermal model described above is nonlinear, a number of simplifications are made when considering the linear model:

- The heat transfer coefficients (h^k_s) do not depend on the actual solid and air temperatures.
- The radiative heat transfer rates are linearized around their current working points into terms of linear radiation coefficients, similar to the convection rates.
- The ventilation flow rates calculated in (1) are determined in terms of the outdoor and reference temperature T_{ref} instead of the transient indoor temperature state T^k_{i}.

The flowchart shown in Figure 2 displays the centralized nonlinear MPC (NLMPC) scheme. The full prediction model is constructed out of prediction functions, with each function representing the thermal model for one of the prediction steps of the receding prediction horizon, N_{p}. Each function is adjusted for each prediction step by considering a new set of time, occupation, ground temperature, weather data and input

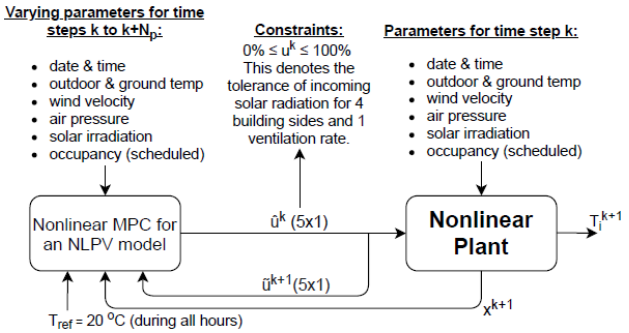

Fig. 2: Centralized nonlinear MPC (NLMPC)

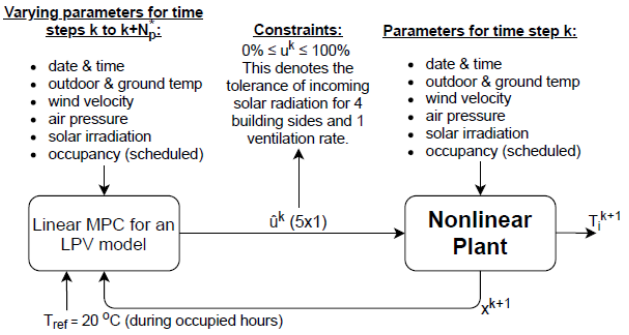

Fig. 3: Centralized Linear MPC (LMPC)

dependent model states from the previous prediction function. The optimization algorithm, employed by MATLAB function *fmincon*, is active-set, as it shows similar results but faster convergence than interior-point and Sequential Quadratic Programming. The MPC strategy is split in two periods, i.e., daytime, when solar shade control is relevant, and night-time. Such approach optimizes 5 input values (1 for the ventilation and 4 for the shaded walls), where the bounds are all set between 1 and 0, representing 100% and 0%, respectively. During night-time, it is only relevant to control the ventilation input. Note that at each time step k, the initial guess set $\tilde{u}$ is set equal to the optimized inputs $\hat{u}$ of the previous time step.

For linear MPC (LMPC), a faster, quadratic programming optimization algorithm is adopted. In this case, the full prediction model encapsulates all prediction step dependent prediction matrices throughout the receding horizon, N^*_{p}. Each matrix also represents the thermal model which is modified by a new set of time, occupancy, ground temperature and weather data, but not by input dependent states, making the prediction model linear. This model is then inserted into a quadratic cost function with penalizing matrices on the stage and terminal costs, resulting in an augmented matrix. The stage and terminal costs are chosen so that the resulting augmented matrix is symmetric positive definite, and the global optimum is guaranteed when the optimal solution is found. The LMPC structure optimizes 5 inputs which are also bounded between 1 and 0. Figure 3 shows the flowchart for LMPC.

The first hierarchical control structure regarded combines

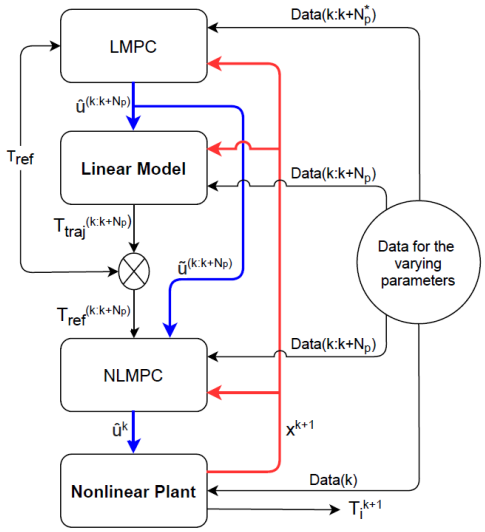

Fig. 4: Hierarchical MPC #1 (HMPC-1)

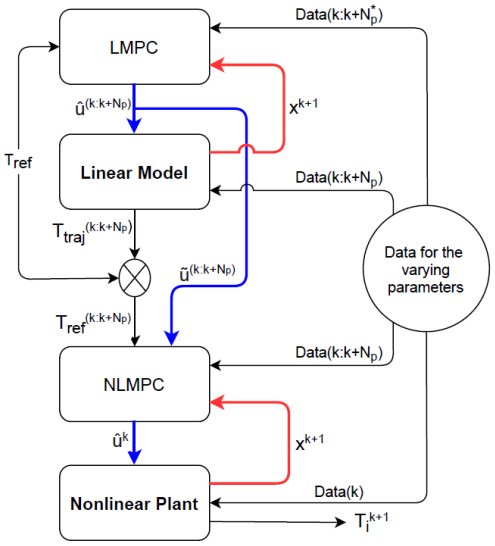

Fig. 5: Hierarchical MPC #2 (HMPC-2)

the main advantages of the last two structures, i.e., it uses linear MPC and the linearized model of the plant to optimize a reference trajectory for the unoccupied hours, T_{traj}, that the nonlinear MPC controller has to track. The control flowchart is illustrated in Figure 4. In this case, the nonlinear plant will be controlled according to the re-optimized input values by the more accurate nonlinear MPC controller. The computation time of the linear controller is low enough to employ easily prediction horizons of 48 prediction steps, while the nonlinear controller does not use a horizon larger than 4, due to heavy computational burdens which increase exponential in relation to the chosen horizon. The choice of horizon is further explained in Section IV.

A second hierarchical structure is introduced to analyze the relevance of the state update strategy, assuming full state knowledge. This is done because the output of the linear model, controlled by linear MPC, could provide better reference trajectories when the two hierarchical layers are separated into their own closed loops. Such MPC flowchart is illustrated in Figure 5.

The third MPC architecture is set forth assuming that the building's heating response due to solar irradiance is relatively slow when compared to the heating response by ventilation. The former response is therefore less sensitive to nonlinearities and the ventilation can compensate quickly with its fast dynamics for thermal errors in the short period. Such approach is illustrated in Figure 6. In this case, the optimal solutions for the input values for the solar shades are applied directly to the nonlinear plant and are not re-optimized by the nonlinear MPC controller. However, they are taken into account by the nonlinear MPC controller for the optimization of the ventilation input. Therefore, the nonlinear MPC controller solely has to optimize the ventilation input, which saves a lot of computation time.

Lastly, a fourth hierarchical MPC structure is developed, according to Figure 7, for the same reason why hierarchical

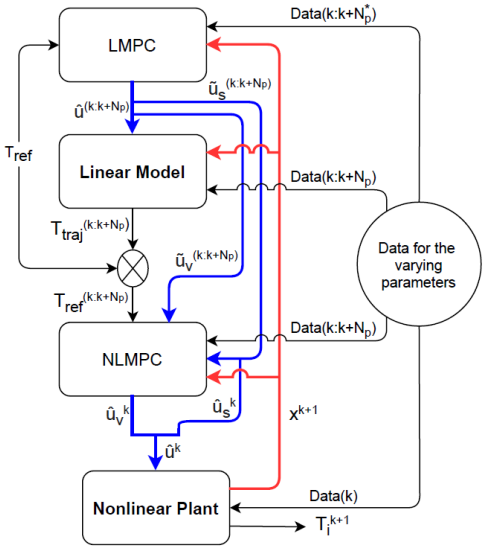

Fig. 6: Hierarchical MPC #3 (HMPC-3)

MPC structure 2 was considered: to analyze the optimal strategy for the state update process.

All five nonlinear MPC controllers presented aim at the minimization of the same objective function, such that

$$\min \sum_{k=1}^{N_{\mathrm{p}}} \left(T_{\mathrm{i}}^{k} - T_{\mathrm{ref}}^{k}\right)^{2} \tag{4}$$

where T_{ref}^{k} is time-dependent and N_{p} the prediction horizon considered. In addition, the non-convexity of the nonlinear optimization problems has been analyzed by integrating a multi-start approach with 40 random initial input guesses in the optimization algorithms.

IV. Results and Discussion

The six MPC architectures were assessed in terms of attending the variance minimization with the reference values,

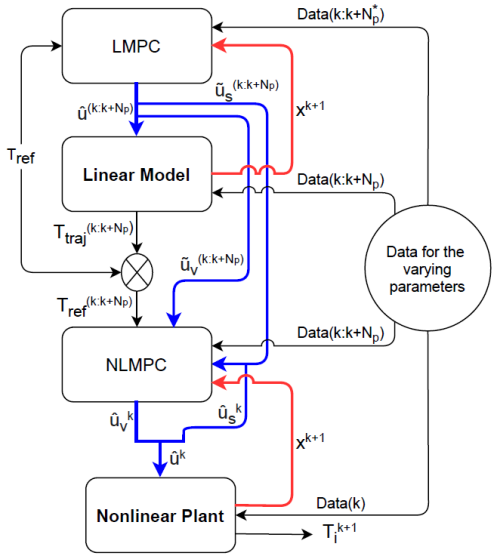

Fig. 7: Hierarchical MPC #4 (HMPC-4)

TABLE II: Results of the MPC structures: $\Delta t = 3600\,\mathrm{s}$

Architecture	N_p	Squared error	Absolute error	Processing time per Δt
NLMPC	8	$313\,^\circ\mathrm{C}^2$	$149\,^\circ\mathrm{C}$	21.1 s
LMPC	24	-14.1%	$+1.3\%$	-99.0%
HMPC-1	4[b]	-15.0%	-9.3%	-76.9%
HMPC-2	4[b]	-11.8%	-8.1%	-75.0%
HMPC-3	4[b]	-20.8%	-12.8%	-92.6%
HMPC-4	4[b]	-20.1%	-12.1%	-92.5%

[b] N_p^* is 24 for the linear block inside the HMPC architecture.

as expressed by the objective function and computation time spent. The results are obtained during occupied hours for 40 days over the early spring. The prediction horizons N_p used, and the results dependent on the chosen control time step Δt, are summarized in Tables II and III. The percentages indicate the degree of improvement per structure with respect to the NLMPC structure, e.g., the absolute error of HMPC-1 is $135\,^\circ\mathrm{C}$ which is an improvement of -9.3% compared to the $149\,^\circ\mathrm{C}$ of the NLMPC architecture.

Even though NLMPC holds the most representative dynamics of the actual plant, the current analysis shows that its control performance is impaired by computational requirements. For instance, the nonlinear controller requires a prediction horizon that should bridge at least the unoccupied period in order to find optimal solutions which take into account the disturbance knowledge of the unoccupied and next occupied periods. Otherwise, the controller will not make preparatory decisions, benefiting that next occupied period. The unoccupied period is assumed to be 16 hours long. This implies, depending on the control time step of 60 or 30 minutes, that a minimum horizon of 17 to 33 prediction steps is required. When the horizon is doubled, the computation time is multiplied by 5.5 to 6. With a standard

TABLE III: Results of the MPC structures: $\Delta t = 1800\,\mathrm{s}$

Architecture	N_p	Squared error	Absolute error	Processing time per Δt
NLMPC	8	$342\,^\circ\mathrm{C}^2$	$146\,^\circ\mathrm{C}$	31.2 s
LMPC	48	-24.3%	-0.7%	-97.7%
HMPC-1	4[c]	-3.5%	-6.2%	-76.5%
HMPC-2	4[c]	-1.5%	-5.5%	-74.5%
HMPC-3	4[c]	-26.0%	-14.4%	-92.1%
HMPC-4	4[c]	-26.3%	-14.4%	-92.5%

[c] N_p^* is 48 for the linear block inside the HMPC architecture.

Intel computer and MATLAB, one time step with a horizon of 17 takes 2 to 3 minutes to solve the NLMPC optimization problem. However, such an MPC controller has minimal information about the next day and operates hourly. It is more preferable to have a longer horizon, such that more information about the next day is included in the optimization problem, and to have a control time step of 30 minutes or even shorter. In this case, the computation time will approach 20 minutes per time step. Full-fledged MPC controllers should have plug-and-play capabilities to accommodate more actuators, e.g., PCM, heat pumps, and operational windows. In that case, the computation time will surpass the control time step, making on-line control impossible. Therefore, it was noted that when the horizon cannot be increased to bridge the unoccupied period, it is better to set N_p at 8 and track the $20\,^\circ\mathrm{C}$ reference temperature during all hours, even if the building is unoccupied. In this case, the system makes no preparatory decisions for future occupied periods, but tries to hold $20\,^\circ\mathrm{C}$. Therefore, the NLMPC structure experiences the largest errors and it is used as benchmark for the other architectures.

For LMPC, the computation time is much lower, while employing a larger horizon. It was noted that when the horizon is doubled, the computation time to solve the LMPC optimization problem increases by 2 to 2.5 times. The horizon thus can easily be set to 24 or even 48 prediction steps. The controller can therefore choose optimal control inputs for the dynamics of the building, which benefits the performance of both the current and next day. The performance in terms of the squared error is significantly improved, but the absolute error results show no improvement. This indicates that the variance of the errors has decreased, but the mean of the errors is increased with respect to the results of the NLMPC structure. This can be explained by the mismatch between the linear prediction model and the nonlinear plant, resulting in small errors and oscillations around the $20\,^\circ\mathrm{C}$ reference temperature.

Regarding the hierarchical structures, in general the algorithms demonstrate lower processing times, due to a lower employed prediction horizon, but also improved performance with respect to the NLMPC structure. Moreover, they are more accurate structures than the LMPC structure, resulting in smaller errors and less oscillations and thus better

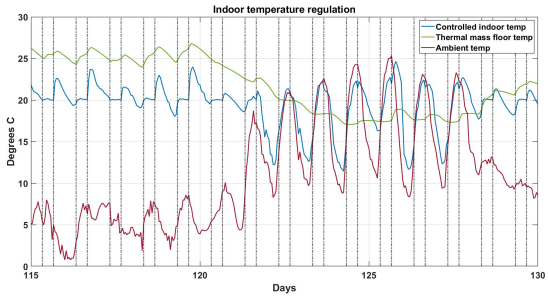

Fig. 8: Performance of HMPC-3 with a 20 °C reference temperature during occupied hours

performance. The higher accuracy is due to the nonlinear MPC lower slave layer that overrules the solutions of the linear MPC higher agent layer, while respecting the optimal reference trajectory. Note that when the nonlinear slave re-optimizes the solutions of the linear agent, which employs a horizon of 24 or 48, it does so with disturbance knowledge of the shorter receding future, as the prediction horizon of the slave controller is set at 4. The results showed that, in case of HMPC-1 and HMPC-2, over the shorter period, the nonlinear slave prefers the ventilation to control the indoor temperature over that of the shading control, since the transient response is faster. However, the shades have a significant effect over a longer period, because they have a large influence on the thermal mass of the floor, which can be beneficial on later notice. For instance, the HMPC-1 structure may prioritize to open the shades and fully use the ventilation in order to cool down the indoor air during a semi-hot day. However, when even warmer weather follows, a better solution might have been to close the shades and make less use of ventilation. This is a scenario that can occur when the shading operations are re-optimized on a shorter future of disturbance knowledge. Additionally, the performances of HMPC-1 and HMPC-2 are comparable, with slightly better results for HMPC-1.

Meanwhile, HMPC-3 seems to solve the problem of HMPC-1 and HMPC-2 regarding the optimal control solutions of the thermal mass by the solar shading. HMPC-3 increases the system's performance by 4% to 9%, depending on the control time step, with respect to HMPC-1. The processing time of HMPC-3 is 68% faster than HMPC-1 and HMPC-2. Therefore, despite its complex structure, this control structure seems to be the best option so far analyzed, while the HMPC-4 architecture does not seem to increase the system's performance significantly.

Figure 8 presents the performance of HMPC-3 over 15 days during April and May. The occupied periods are indicated by vertical dotted lines. The figure shows clearly that the building prepares itself for the next day, e.g., during the cold period, it heats the indoor air (blue line) up after the occupied period has ended and during the hot period, it tries to cool down the thermal mass of the floor (green line) as much as possible during the night.

V. Conclusions

This work has investigated effective MPC methods to optimize the integration of a thermal chimney and a solar shading system for passive HVAC of an office building at the TU Delft campus. Six architectures were tested, including a linear and nonlinear approach, and four hierarchical variants. The results indicate that the hierarchical architecture HMPC-3 presents promising performance. The advantages of this architecture can be explained by the separation of controllable actuators, based on their effect on the dynamical system, into distinct control strategies, suppressing the computation time.

On-going and future work include the analyze of other computational demand reducing methods for MPC, e.g., shorten the control horizon relative to the prediction horizon and applying more efficient nonlinear solvers, like IPOPT.

References

[1] European Commission, "Mapping and analyses of the current and future (2020-2030) heating/cooling fuel deployment (fossil/renewables)", 2016.

[2] X. Cao, X. Dai and J. Liu, "Building energy-consumption status worldwide and the state-of-the-art technologies for zero-energy buildings during the past decade", *Energy and Buildings,* pp. 198-213, 2016.

[3] J. Drgoňa et al., "All you need to know about model predictive control for buildings", *Annual Reviews in Control*, pp. 190-232, 2020.

[4] M. Tanaskovic et al., "Robust adaptive model predictive building climate control", *IFAC-PapersOnLine*, pp. 1871-1876, 2017.

[5] A. Parisio et al., "A scenario-based predictive control approach to building HVAC management systems", *IEEE International Conference on Automation Science and Engineering*, pp. 428–435, 2013.

[6] J. Drgoňa et al., "Explicit stochastic MPC approach to building temperature control", *IEEE Conference on Decision and Control*, pp. 6440-6445, 2013.

[7] S. Koehler and F. Borrelli, "Building temperature distributed control via explicit MPC and trim and respond methods", *European Control Conference*, pp. 4334-4339, 2013.

[8] H. Scherer et al., "Efficient building energy management using distributed model predictive control", *Journal of Process Control*, pp.740-749, 2014.

[9] V. Putta et al., "Distributed model predictive control for building HVAC systems: A case study", *International High Performance Buildings Conference*, pp. 3611-3619, 2014.

[10] Y. Long et al., "A hierarchical distributed MPC for HVAC systems", *2016 American Control Conference*, pp. 2385-2390, 2016.

[11] G. Mantovani, L. Ferrarini, and S. Member, "Temperature control of a commercial building with model predictive control techniques", *Transactions on Industrial Electronic*, pp. 2651-2660, 2015.

[12] M. Maasoumy and A. Sangiovanni-Vincentelli, "Total and peak energy consumption minimization of build-

ing HVAC systems using model predictive control", *Design and Test of Computers*, pp. 26–35, 2012.

[13] Y. Ma, J. Matusko, and F. Borrelli, "Stochastic model predictive control for building HVAC systems: Complexity and conservatism," *Transactions on Control Systems Technology*, pp. 101–116, 2015.

[14] ANSYS, "GRANTA EduPack, Formerly CES EduPack: Materials Education Support", www.ansys.com/products/materials/granta-edupack, Accessed on January 15, 2020.

[15] T. L. Bergman et al., "Fundamentals of Heat and Mass Transfer", New York: *John Wiley & Sons*, 2011.

[16] KNMI, "Soil Temperatures", www.knmi.nl/nederland-nu/klimatologie/bodemtemperaturen, Accessed on January 15, 2021.

[17] J. Duffie and W. Beckman, "Solar Engineering of Thermal Processes", New York: *John Wiley & Sons*, 2013.